Electronic Supplementary Material (ESI) for Journal of Materials Chemistry A.

SUPPORTING INFORMATION

Multifunctional cobalt iron sulfide electrocatalyst for high performance Zn-air battery and overall water splitting

Mukesh Kumar and Tharamani C. Nagaiah*

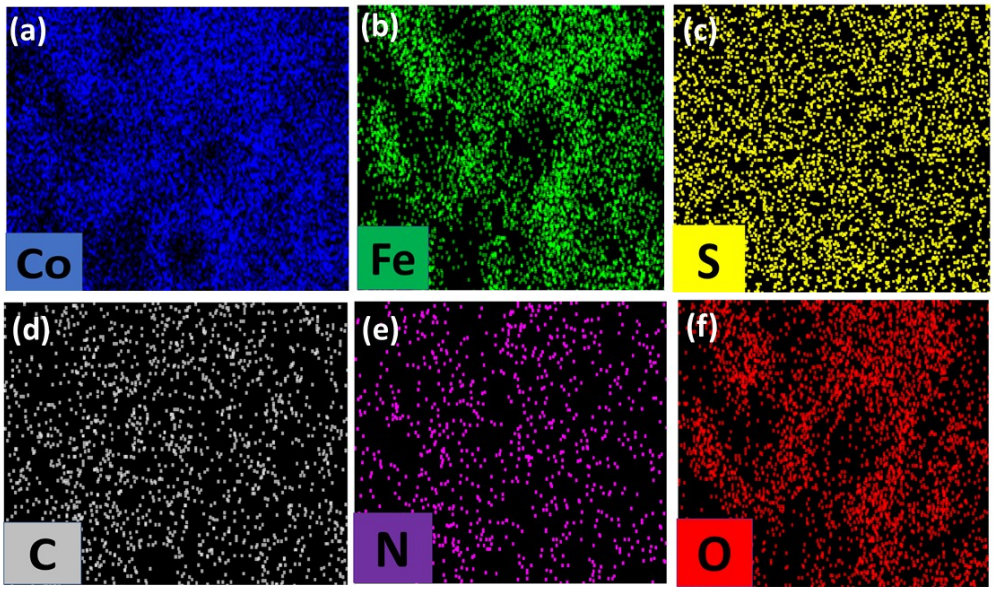

Fig. S1. Elemental dot mapping images representing the distribution of (a) cobalt, (b) iron, (c) sulfur, (d) carbon, (e) nitrogen and (f) oxygen in $CoFe(3:1)S_2$ catalyst.

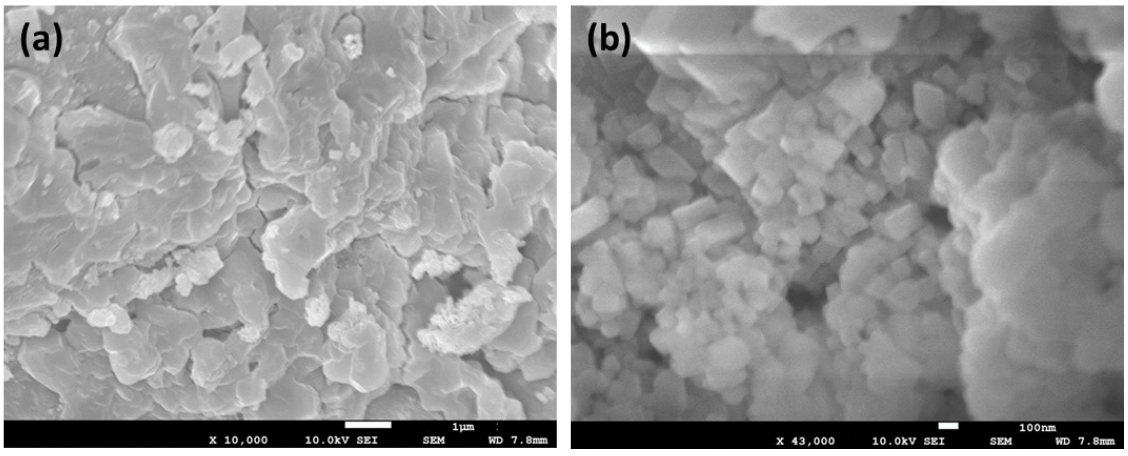

Fig. S2. FE-SEM images of (a) FeS_2 and (b) CoS_2 catalysts.

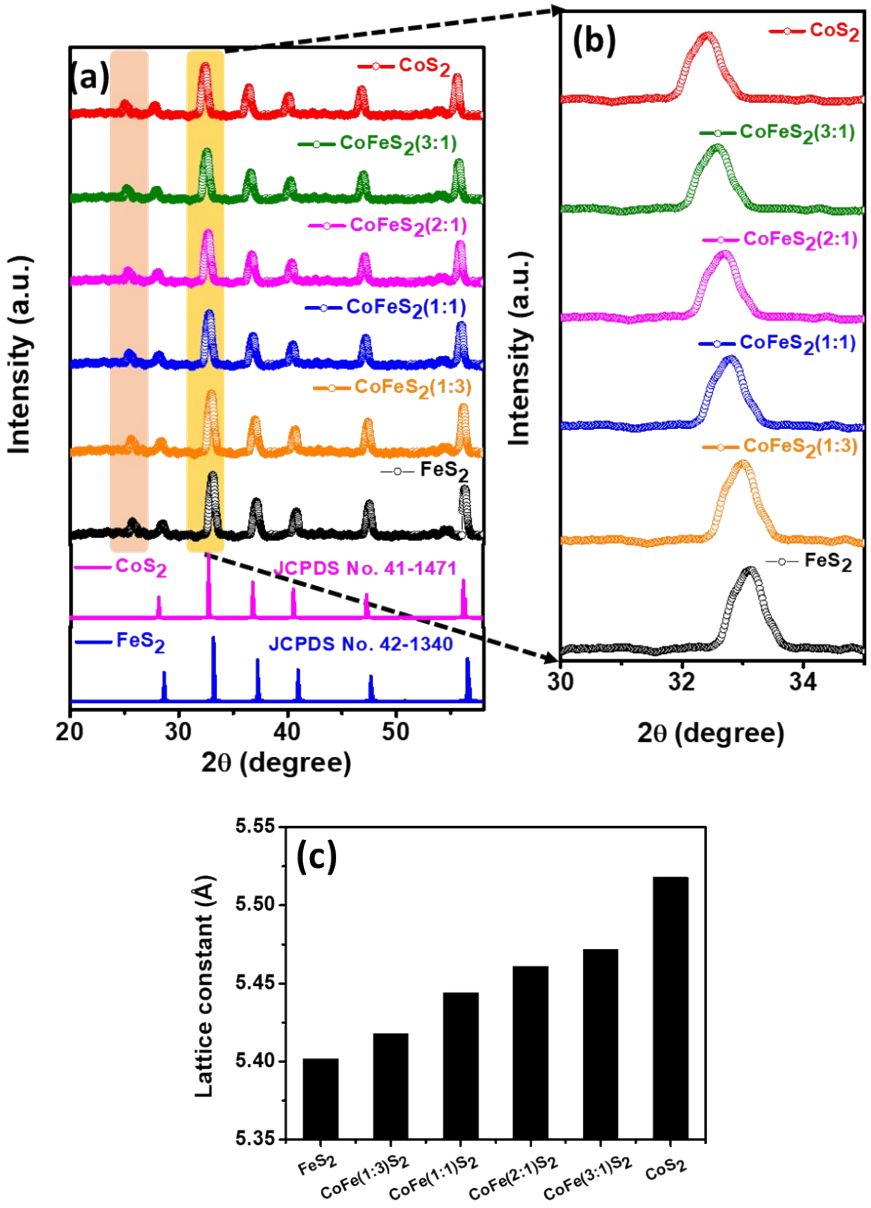

Fig. S3. (a) and (b) XRD pattern of various catalysts and (c) bar diagram representing the average lattice constant of different catalysts.

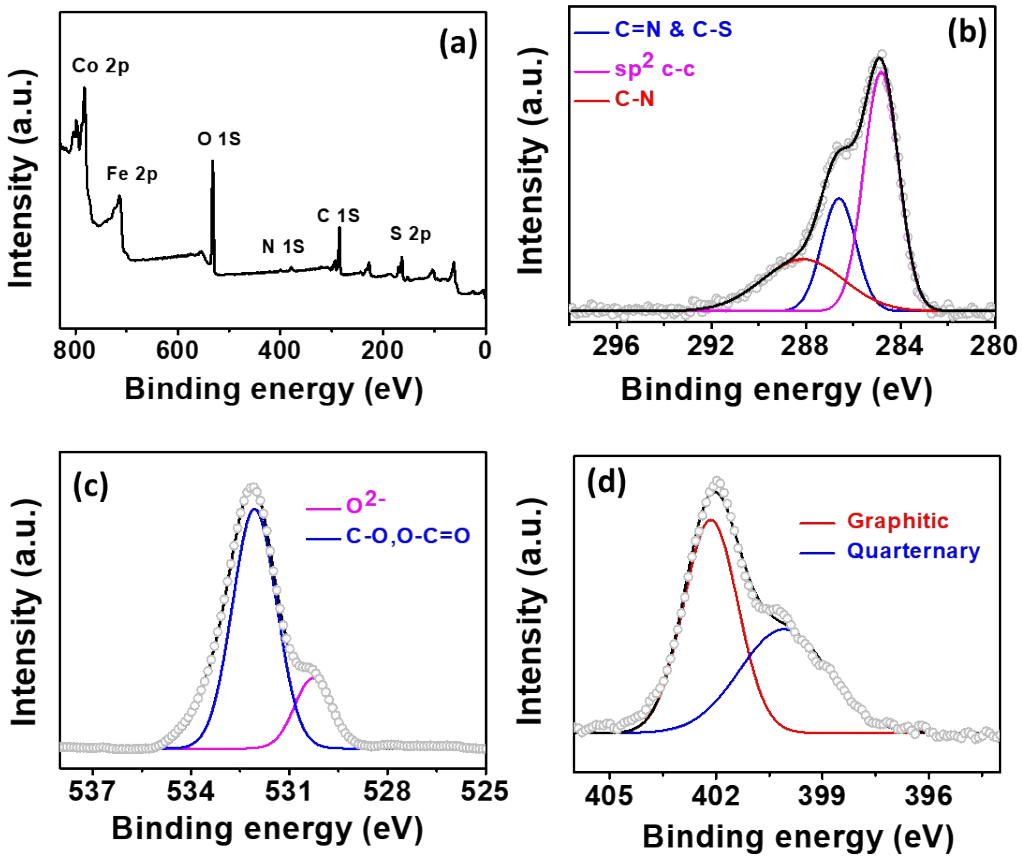

Fig. S4. (a) XPS survey spectrum and deconvoluted XP spectra of (b) C 1s, (c) O 1s, and (d) N 1s, of CoFe(3:1)S_2 catalyst.

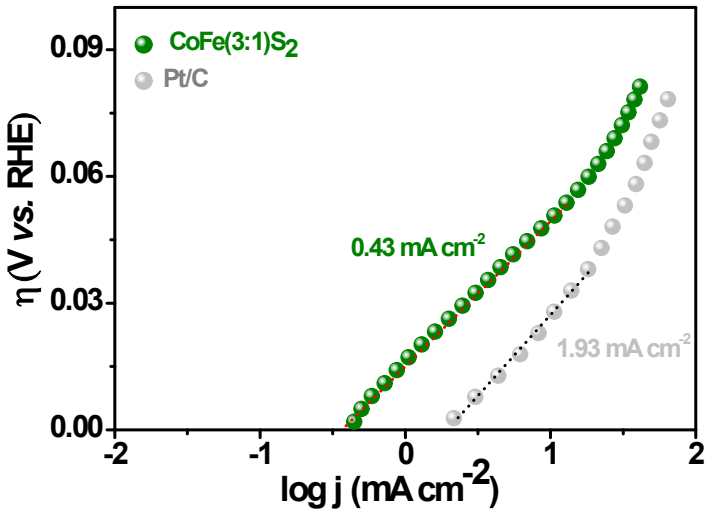

Fig. S5. Exchange current density for CoFe(3:1)S_2 and Pt/C obtained by extraploting Tafel slope.

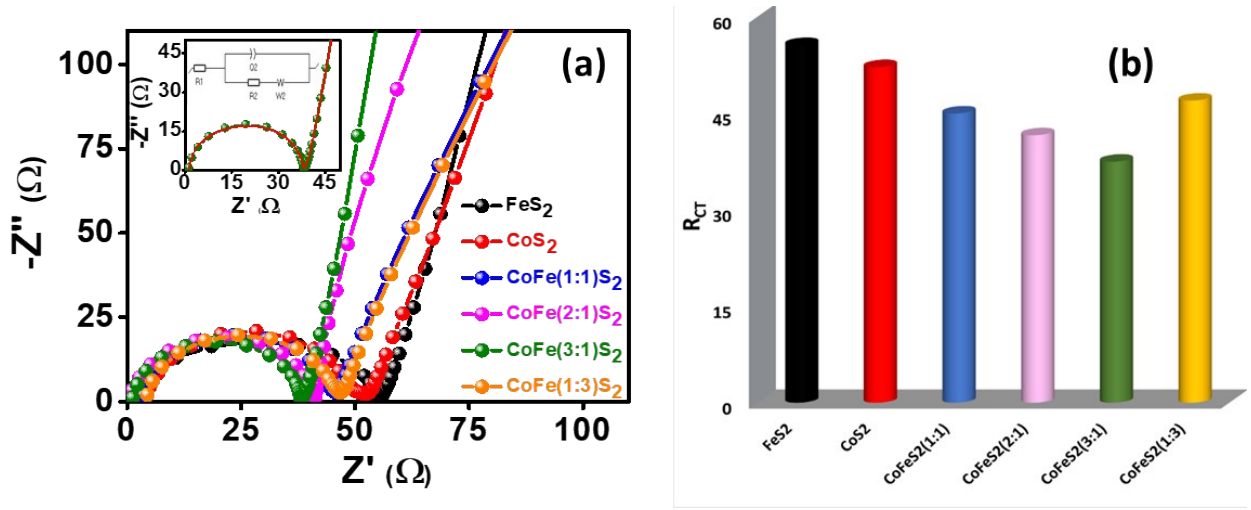

Fig. S6. (a) EIS (b) corresponding charge transfer resistance extracted from Nyquist plot of various catalyst in 0.5 M H_2SO_4 electrolyte, CE: Pt wire, RE: SCE.

Table S1: Electrochemical Impedance analysis extracted from Fig. S6.

Catalysts	R1(Solution resistance)	R2(Polarization resistance)	R_{ct} = R2-R1
FeS_2	3.728	55.2	51.472
CoS_2	5.2	52.4	47.2
$CoFe(1:1)S_2$	3.5	45.9	42.4
$CoFe(2:1)S_2$	2.1	41.02	38.92
$CoFe(3:1)S_2$	1.0	38.36	37.36
$CoFe(1:3)S_2$	4.45	46.80	42.35

Electrochemical surface area (ECSA):

Electrochemical active sites closely interlinked with the superior performance of the electrode material. Therefore, determination of ECSA which is associated with the no of active sites gives us fruitful information regarding the superior performance of catalyst. ECSA was determined by performing the CV at various scan rates (10-300 mVs^{-1}) in the non-faradic region from 0.0 V to 0.5 V. Afterward electrochemical double layer capacitance (C_{dl}) was determined by plotting the average current density ($(I_a+I_c)/2$) *vs.* scan rate. The ECSA is calculated by dividing this slope with specific capacitance (20-60 µF cm^{-2}) of the flat standard surface, in the present study its value is considered to be 40 µF cm^{-2}.[1] As shown in Fig. S8b, the ECSA value is highest for $CoFe(3:1)S_2$, confirming the high electrochemical activity of $CoFe(3:1)S_2$ is due to large no. of exposed electrochemically active sites.

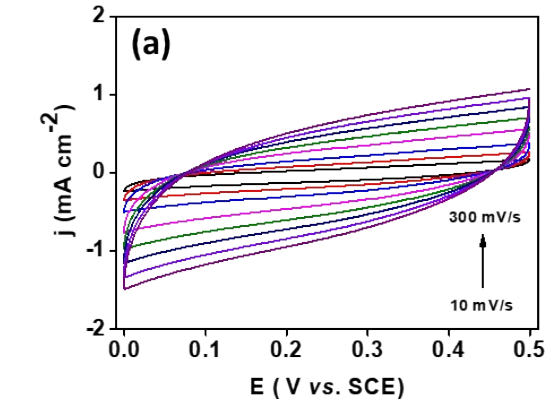
(a)
j (mA cm-2)
300 mV/s
10 mV/s
E (V vs. SCE)

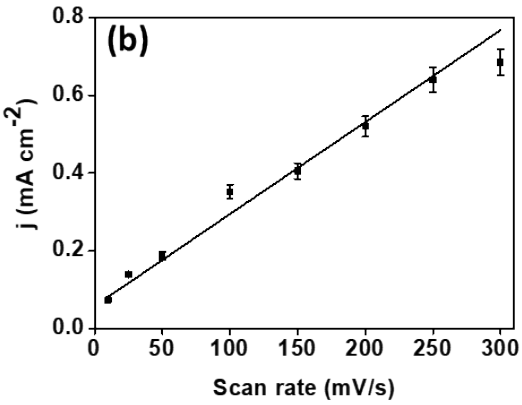
(b)
j (mA cm-2)
Scan rate (mV/s)

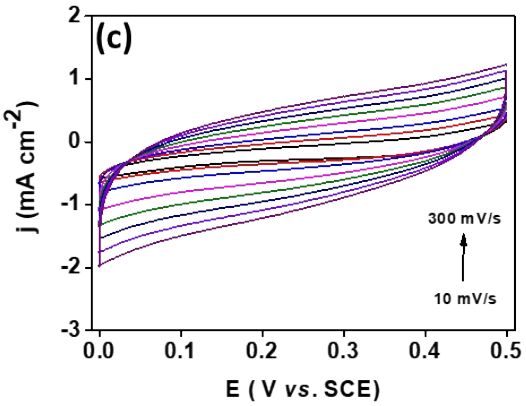
(c)
j (mA cm-2)
300 mV/s
10 mV/s
E (V vs. SCE)

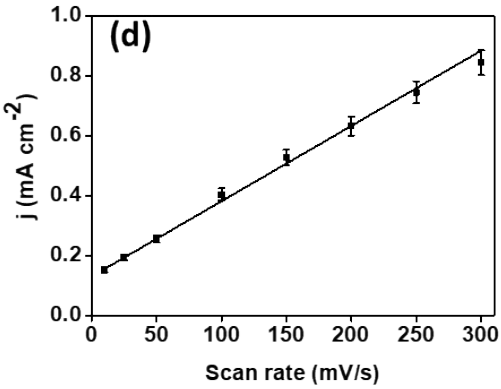
(d)
j (mA cm-2)
Scan rate (mV/s)

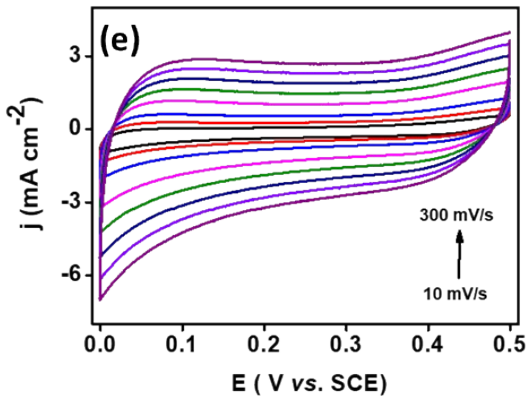
(e)
j (mA cm-2)
300 mV/s
10 mV/s
E (V vs. SCE)

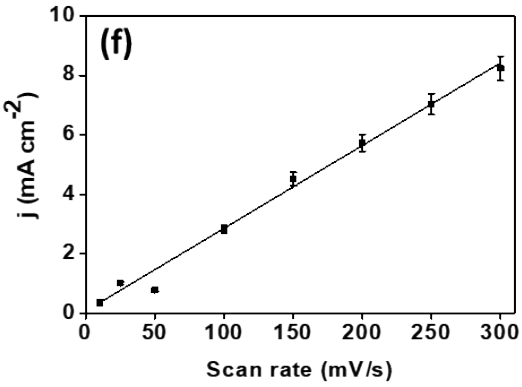
(f)
j (mA cm-2)
Scan rate (mV/s)

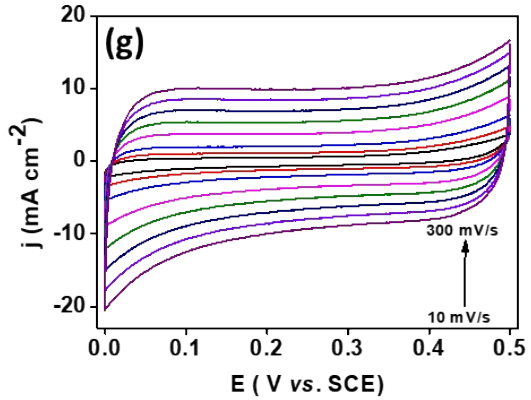
(g)
j (mA cm-2)
300 mV/s
10 mV/s
E (V vs. SCE)

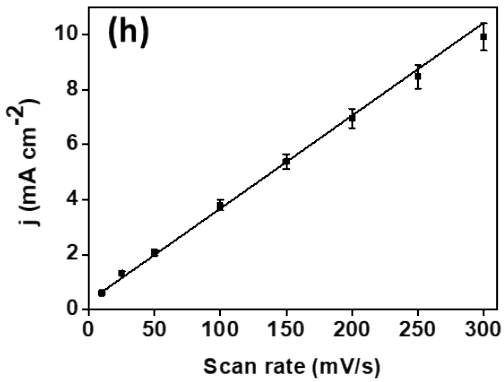
(h)
j (mA cm-2)
Scan rate (mV/s)

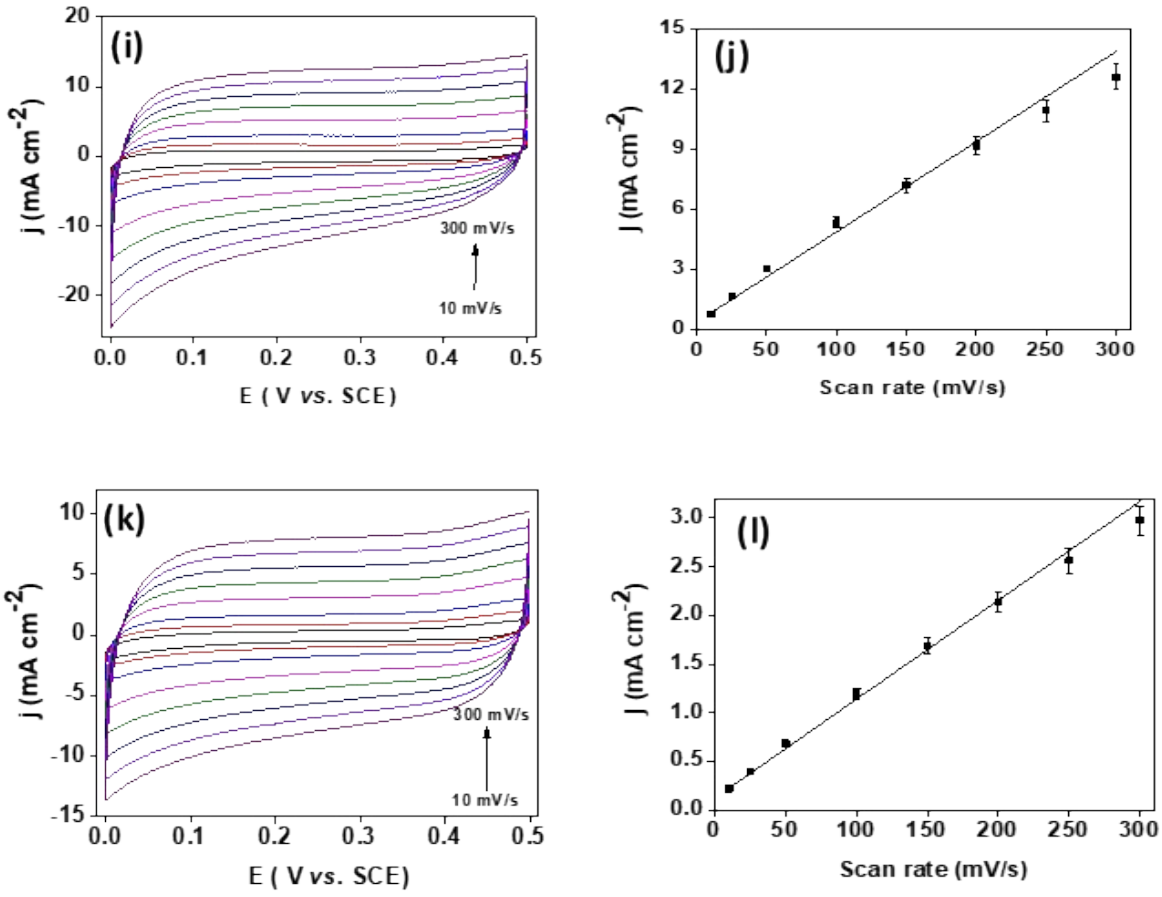

Fig. S7. CVs of (a) FeS_2 , (c) CoS_2 , (e) $CoFe(1:1)S_2$ (g) $CoFe(2:1)S_2$ (i) $CoFe(3:1)S_2$, (k) $CoFe(1:3)S_2$ at various scan rates in the non-faradaic potential region and (b), (d), (f),(h), (j), (l) are corresponding average current versus scan rate plot in 0.5 M H_2SO_4 electrolyte, CE: Pt wire, RE: SCE.

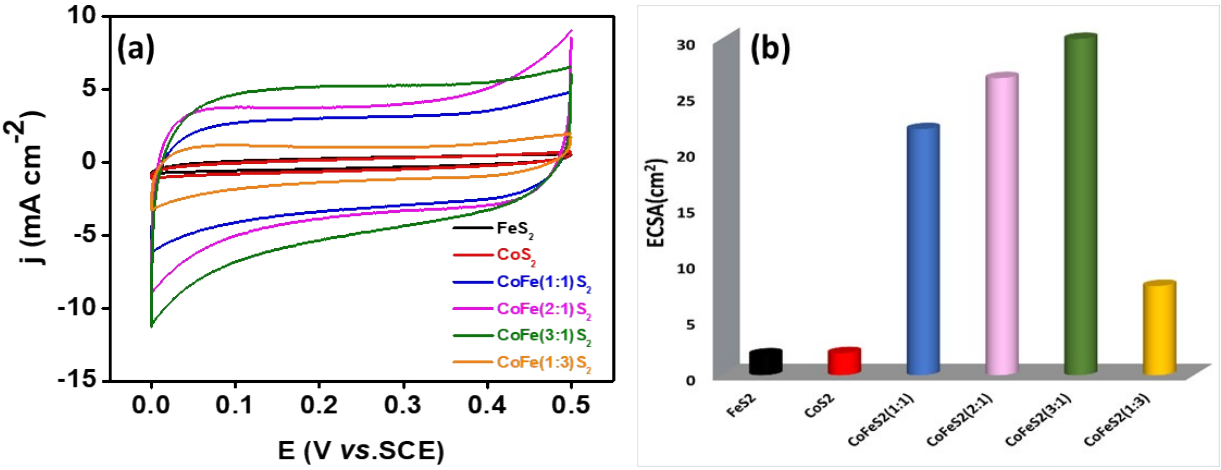

Fig. S8. (a) Comparative CVs at 100 mV s^{-1} and (b) corresponding ECSA of various catalyst in 0.5 M H_2SO_4 electrolyte, CE: Pt wire, RE: SCE.

No. of electrochemical active sites by UPD method :

As shown in Fig. S9a initially CV scan was performed at 2 mV s^{-1} in 0.5 M H_2SO_4 solution which showed no oxidation and reduction peak acts as a baseline. Afterward 20 mM CuSO4 was added to 0.5 M H_2SO_4 and CV was performed under similar condition a clear distinguish peak for OPD, UPD and their stripping peaks can be observed clearly. Looking at CV for CoFe(3:1)S_2 a series of LSV were carried out for stripping of Cu starting from different overpotential Fig. S9b. As shown in Fig. S9b flat region present at 0.0165 C (for CoFe(3:1)S_2 between the 0.205 V to 0.225 V gives us a good measure to calculate the no. of active sites which further normalised with respect to geometric area of electrode (0.0314 cm^2).For comparison the no of sites for CoS_2 and FeS_2 were also calculated under similar condition following same procedure

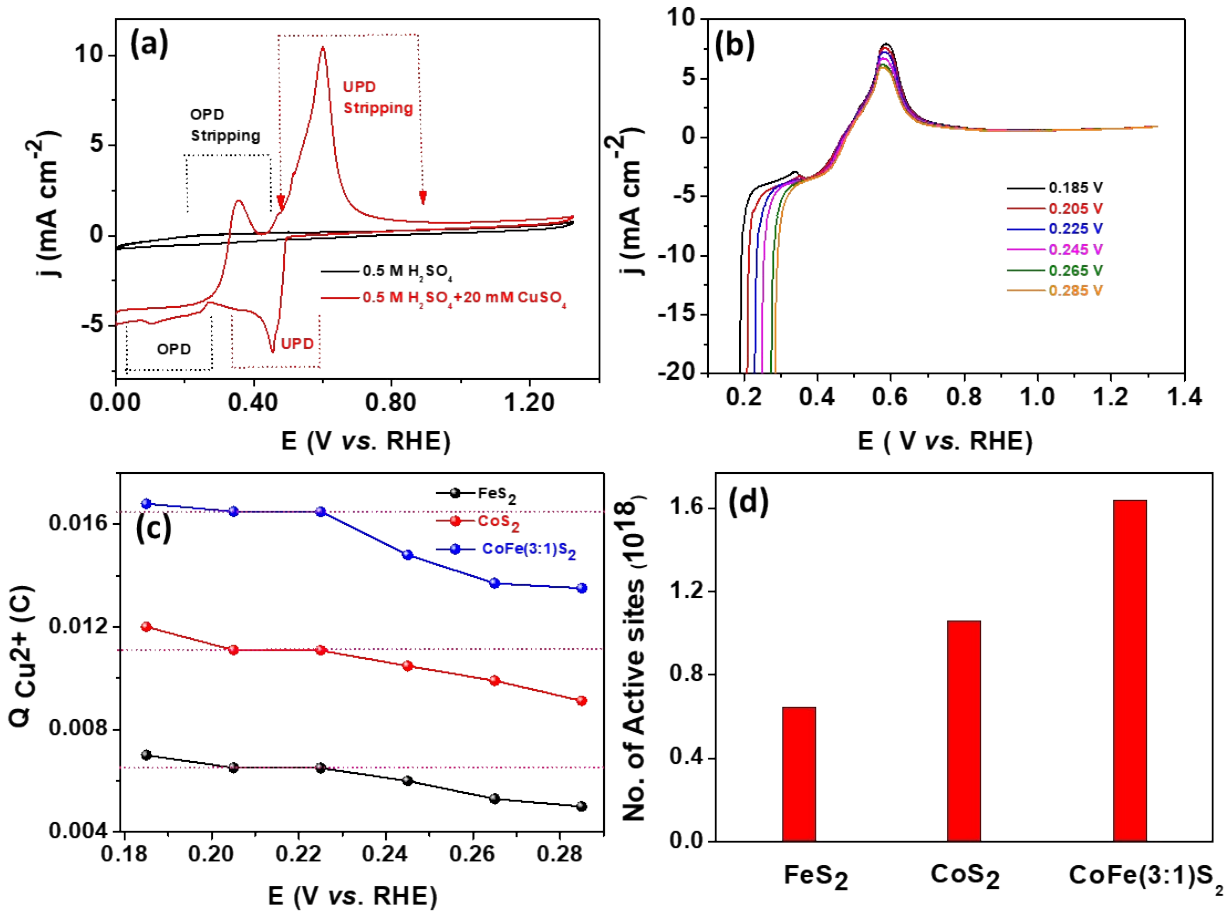

Fig. S9. (a) CVs of CoFe(3:1)S_2 with and without $CuSO_4$ (b) LSVs of CoFe(3:1)S_2 under different starting voltages, (c) charges required to strip the Cu deposited at different underpotentials, (d) no. of active sites of various catalysts.

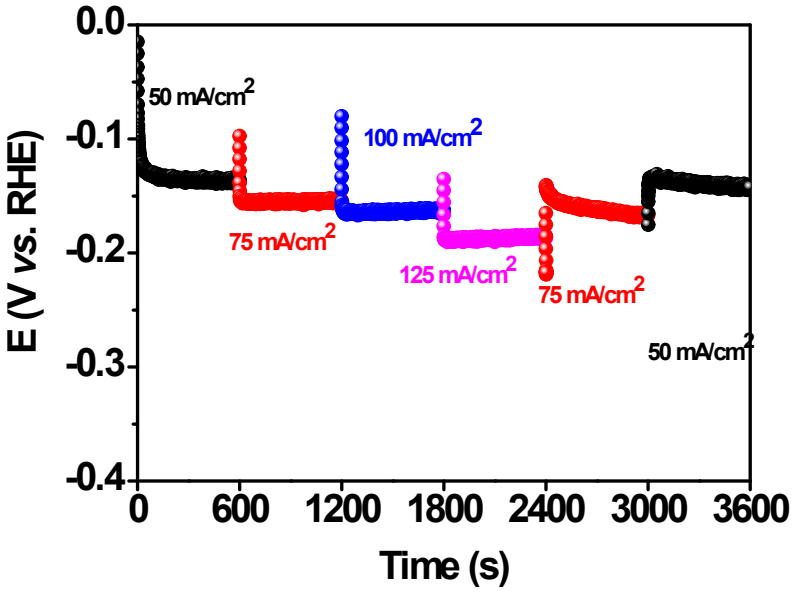

Fig. S10. Sequential chronopotentiometry study for CoFe(3:1)S_2 at various current density in 1 M KOH electrolyte, CE: Pt-wire, RE: Hg/HgO/1 M NaOH.

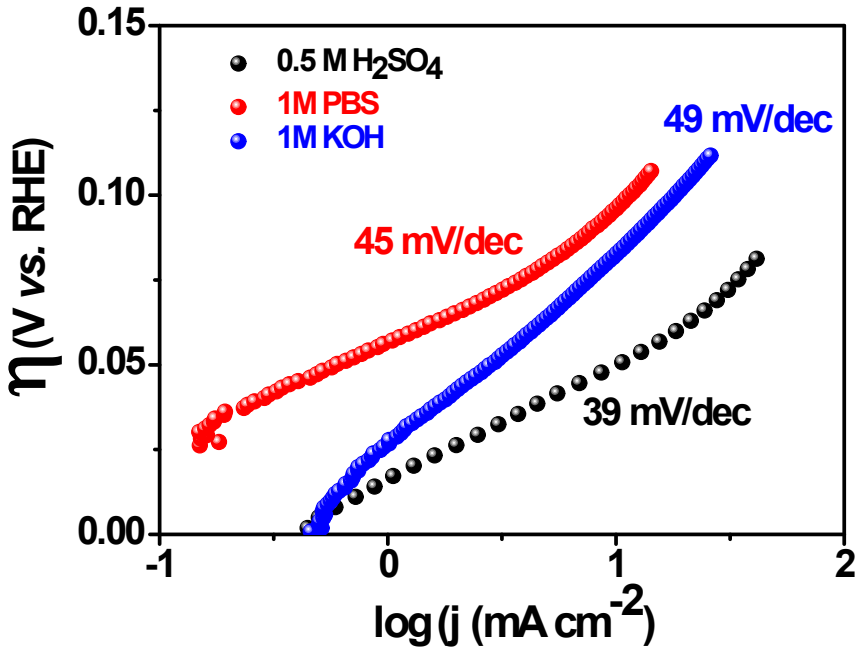

Fig. S11. Tafel plot of CoFe(3:1)S_2 in various electrolyte extracted from Fig. 2e (main manuscript).

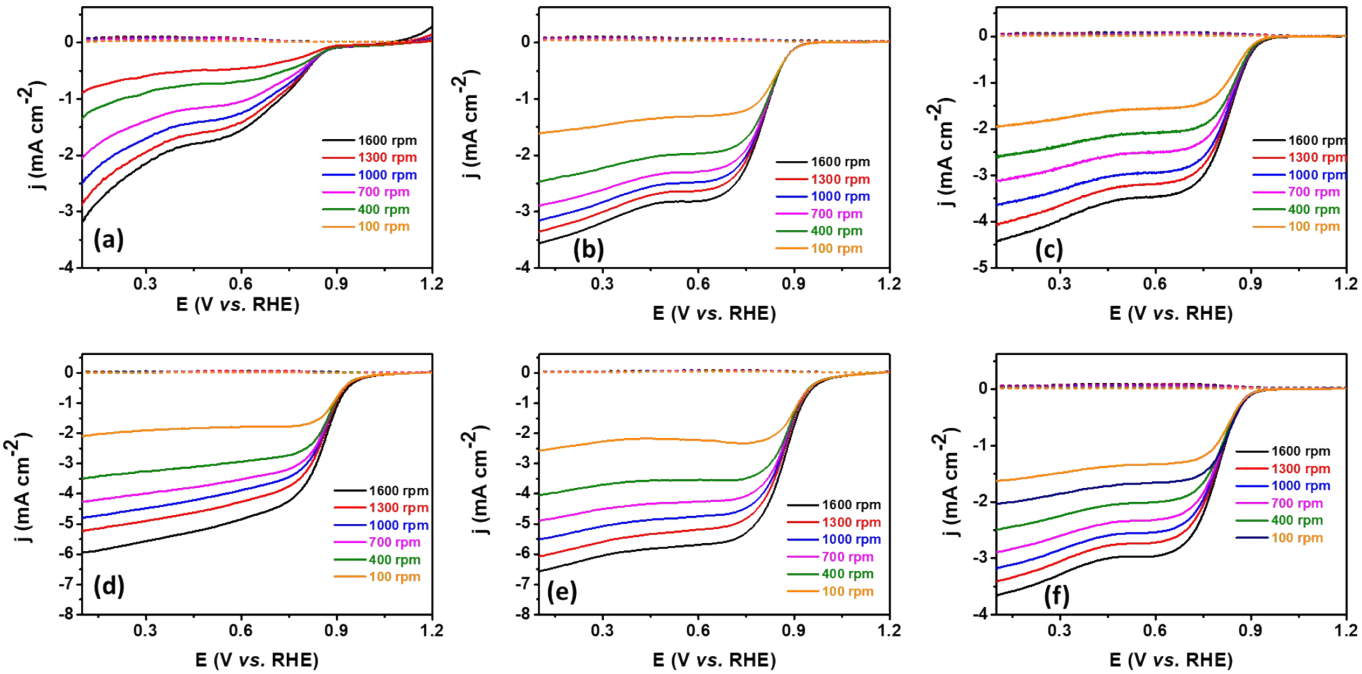

Fig. S12. RRDE Linear polarization curves for (a) FeS_2, (b) CoS_2, (c) $CoFe(1:1)S_2$,(d) $CoFe(2:1)S_2$, (e) $CoFe(3:1)S_2$,and (f) $CoFe(1:3)S_2$ at varying rotation rates in 0.1 M KOH at a scan rate of 5 mV s^{-1}. CE: Pt-wire; RE: Hg/HgO/1 M NaOH.

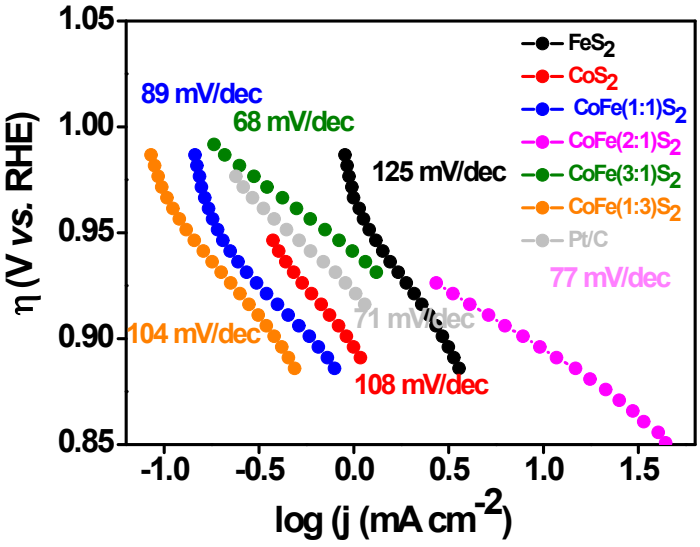

Fig. S13. Tafel plot of various catalysts extracted from Fig. 3b (main manuscript).

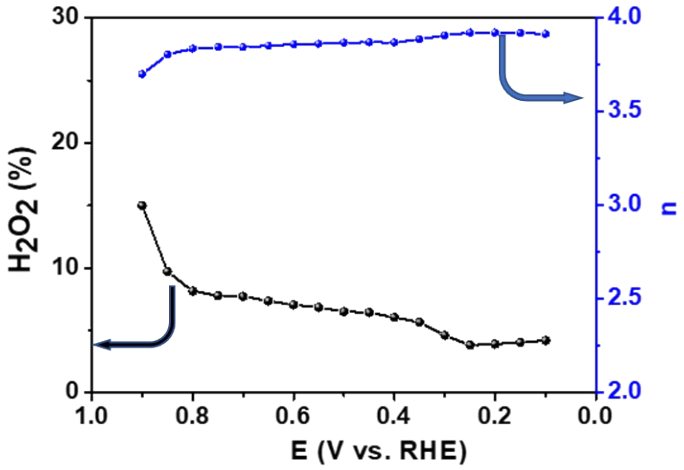

Fig. S14. No. of electron and amount of H_2O_2 produced at various potentials for CoFe(3:1)S_2.

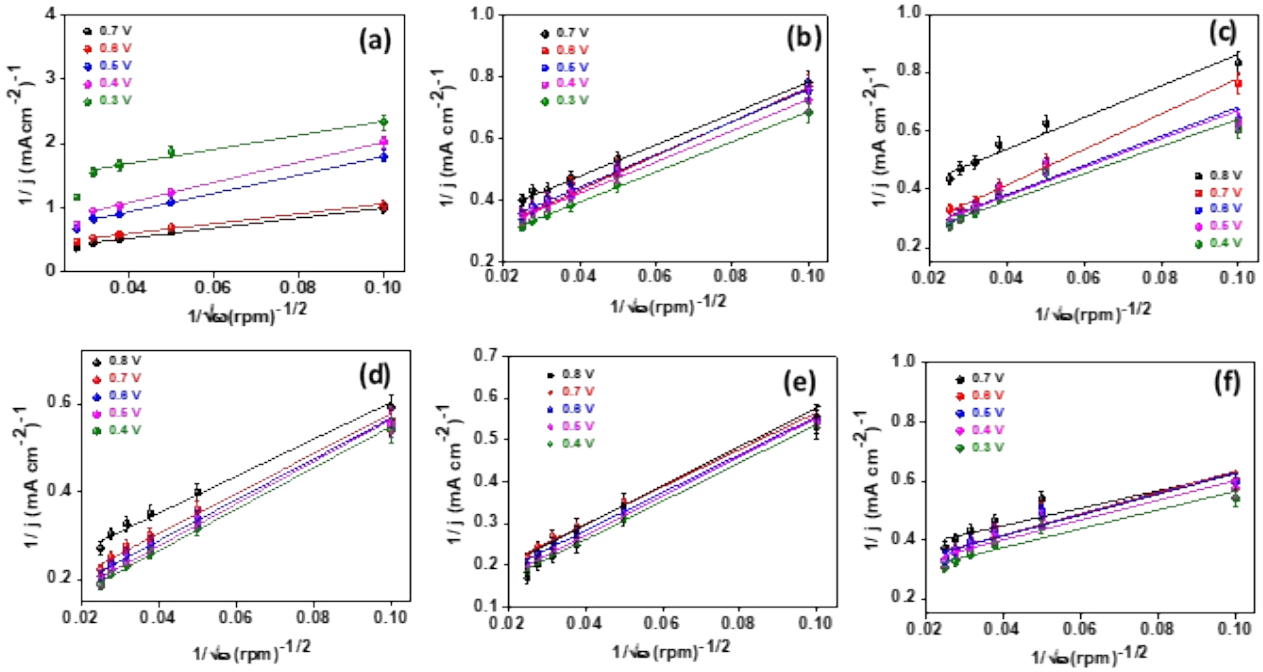

Fig. S15. Koutecky-Levich (K-L) plot for (a) FeS_2, (b) CoS_2, (c) CoFe(1:1)S_2,(d) CoFe(2:1)S_2, (e) CoFe(3:1)S_2, and (f) CoFe(1:3)S_2 at various potential extracted from the linear polarisation curve at various rotation rates in 0.1 M KOH at a scan rate of 5 mV s^{-1}. CE: Pt-wire; RE: Hg/HgO/1 M NaOH.

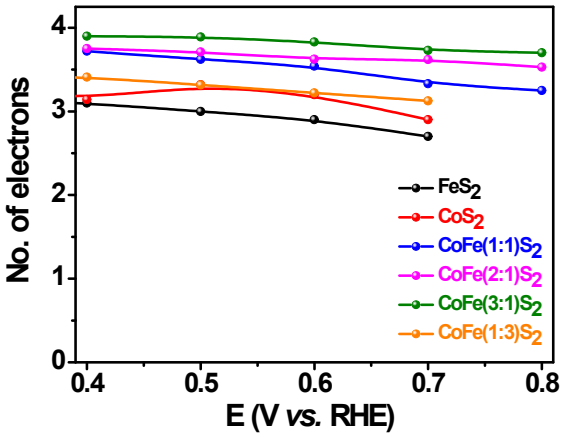

Fig. S16. Potential dependent number of electron extracted from RDE plot in 0.1 M KOH at a scan rate of 5 mV s^{-1}. CE: Pt wire; RE: Hg/HgO/1 M NaOH.

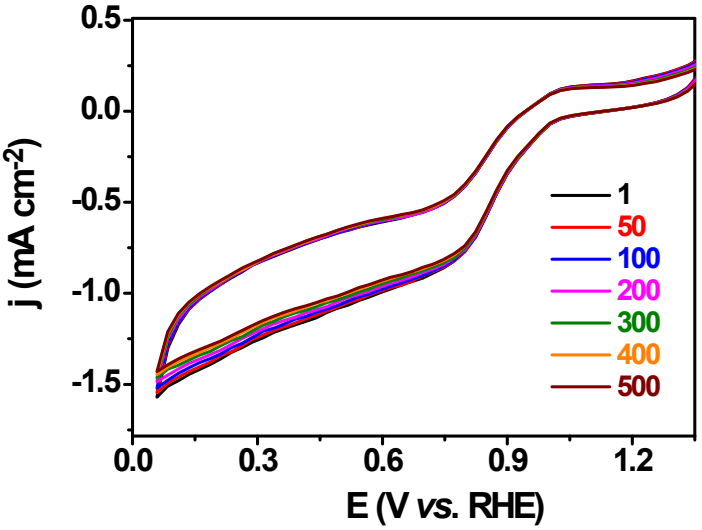

Fig. S17. CVs for CoFe(3:1)S_2 in oxygen saturated 0.1 M KOH upto 500 cycles at a scan rate of 25 mV s^{-1} CE: Pt wire, RE: Hg/HgO/1 M NaOH.

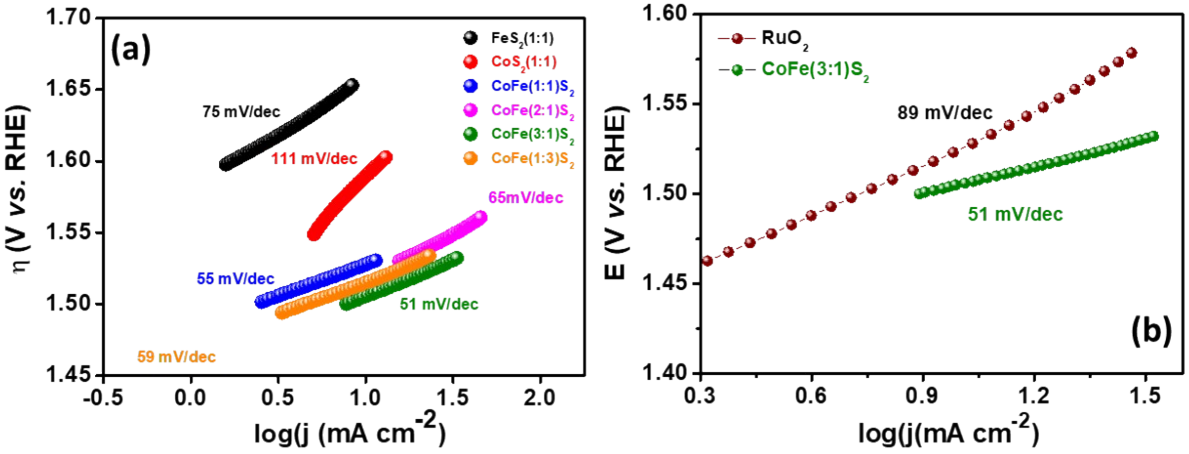

Fig. S18. (a) and (b) are the Tafel plot extracted from linear polarisation curves of Fig. 6a main graph recorded in 0.1 M KOH at a scan rate of 5 mV s^{-1}, CE: Pt wire, RE: Hg/HgO/1 M NaOH

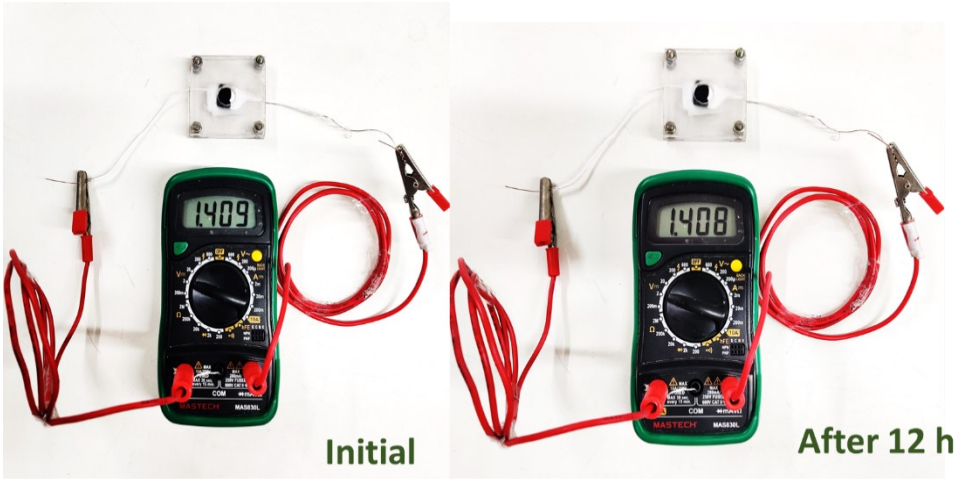

Fig. S19. Photographs of the OCP recorded for a Zn-air battery assembled with CoFe(3:1)S_2 air cathode by a multimeter before and after 12 h.

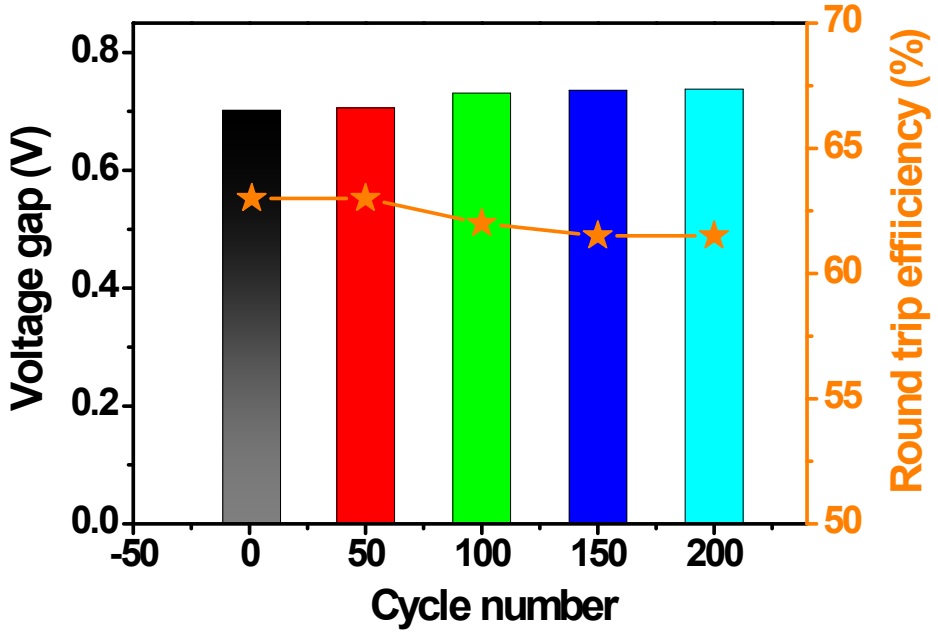

Fig. S20. Bar diagram showing the voltage gap and round trip efficiency (%) recorded during the stability study of a Zn-air battery assembled using CoFe(3:1)S_2 air cathode for 210 cycles.

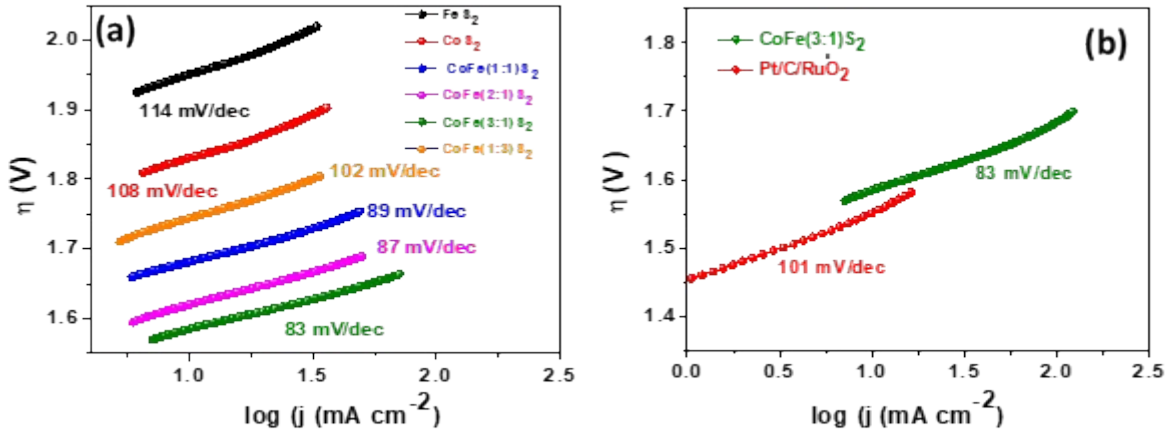

Fig. S21. (a) and (b) are the Tafel plot extracted from linear polarisation curves of Fig. 6a main graph recorded in 1 M KOH at a scan rate of 5 mV s^{-1}, CE: Pt wire, RE: Hg/HgO/1 M NaOH

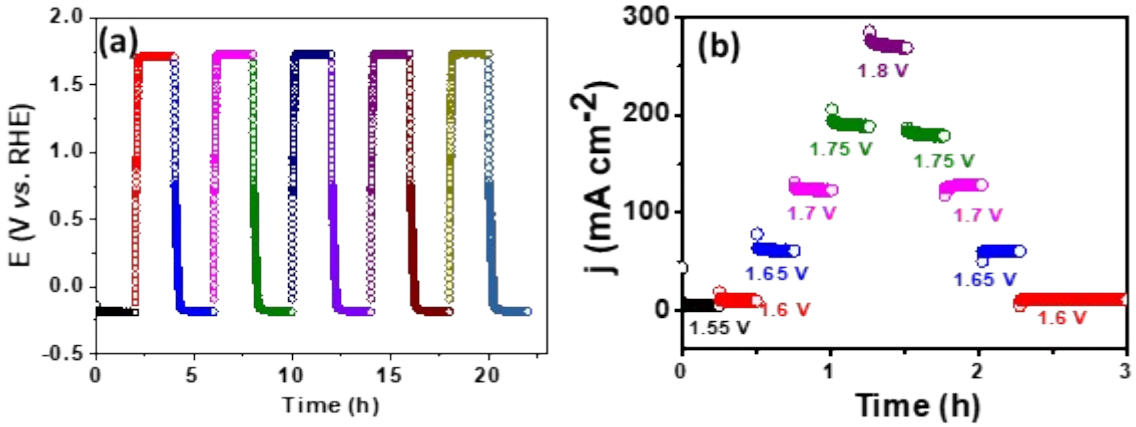

Fig. S22. (a) Chronopotentiometric curve of water splitting device recorded at 100 mA cm^{-2} for OER and -100 cm^{-2} for HER in three electrode system where the polarity of a device was reverse after 30 minutes, (b) multistep chronoamperometric curve of a water splitting device recorded by sweeping the potential from 1.55 V to 1.8 V.

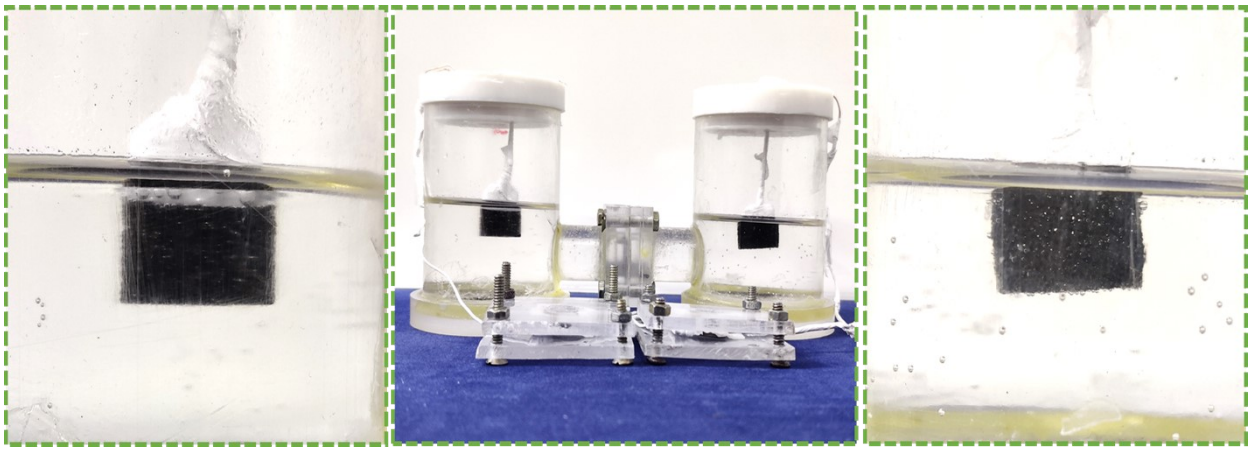

Fig. S23. (a) Photograph of overall water splitting driven by two Zn-air batteries assembled in a series using CoFe(3:1)S_2 air cathode.

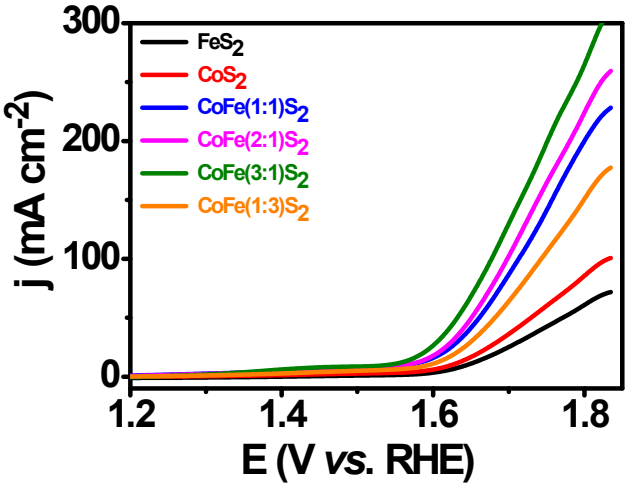

Fig. S24 LSVs of various catalysts in 0.5 M H_2SO_4 at 5 mV s^{-1} representing the OER activity of various catalysts,

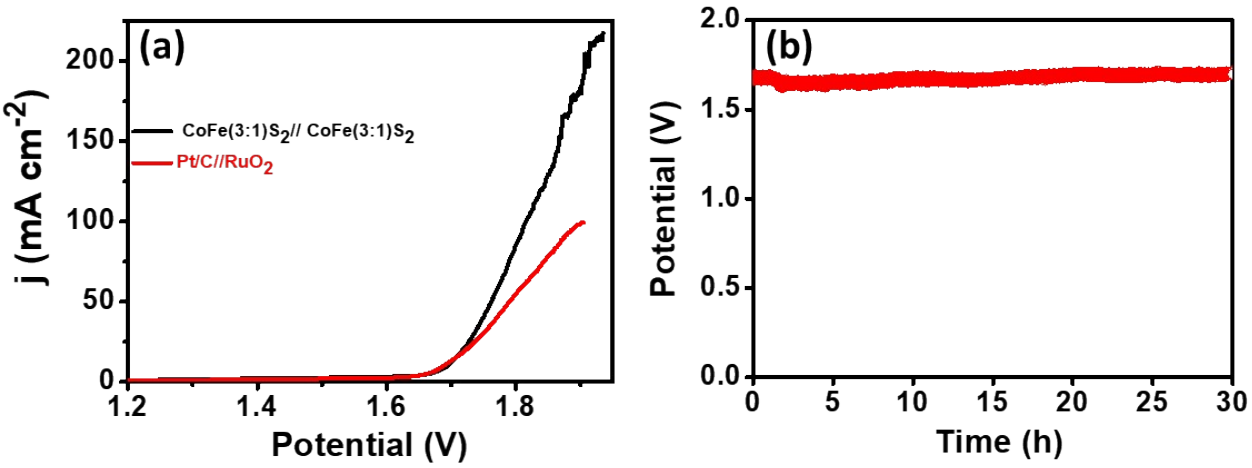

Fig. S25. (a) Comparative LSVs of $CoFe(3:1)S_2$ with state of art catalyst for water splitting at 5 mV s^{-1}, (b) chronopotentiometric curve recorded at 10 mA cm^{-2} for $CoFe(3:1)S_2$ under overall water splitting in 0.5 M H_2SO_4.

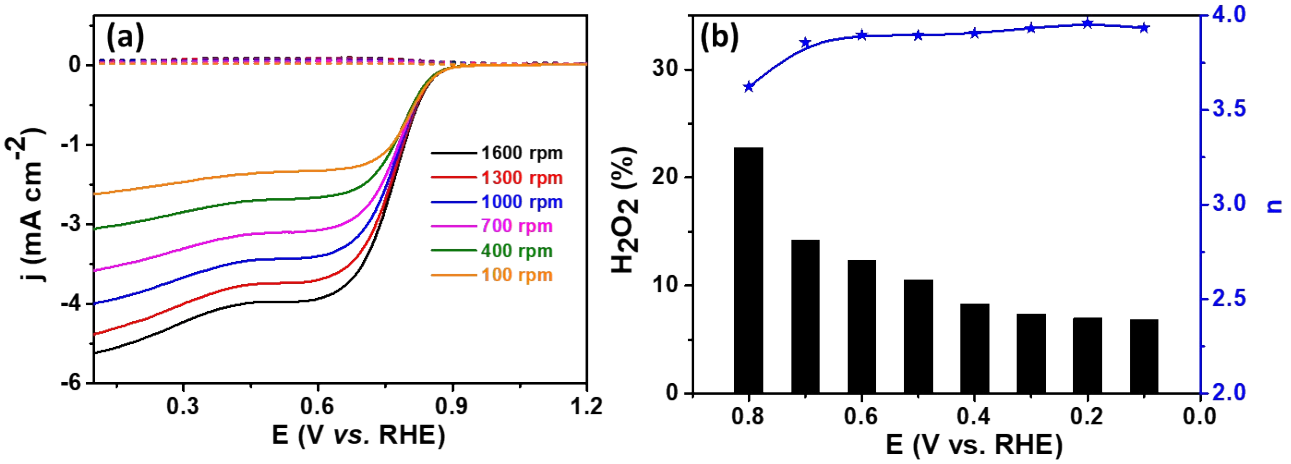

Fig. S26. (a) RRDE polarization curves at 5 mV s^{-1} at various rotation rates, (b) bar diagram representing the no. of electron and % of H_2O_2 at various potentials at 1600 rpm.

All the catalysts show good OER activity validated from the steep increase in the current density. But among all the catalyst CoFe(3:1)S_2 demonstrate the highest OER acitivity with a low overpotential of 306 mV@10 mA cm^{-2} and achieved a high current density of 303 mA cm^{-2} @1.83 V. When CoFe(3:1)S_2 is equipped in water electrolyser, both as anode and cathode reaches a cell voltage of 10 mA cm^{-2} at 1.68 V which is comparable to the benchmark catalysts. Besides, the catalyst also exhibits a good cycling stability indicated by the stable potential response for 30 h at a constant current density of 10 mA cm^{-2}.

Further, the catalyst also shows a good ORR activity in 0.5 M H_2SO_4 with a very good onset potential of 0.92 V vs. RHE and a half-wave potential of 0.77 V *vs.* RHE. The no. of electron was close to the ideal 4 electron and H_2O_2 % was close to 10 %.

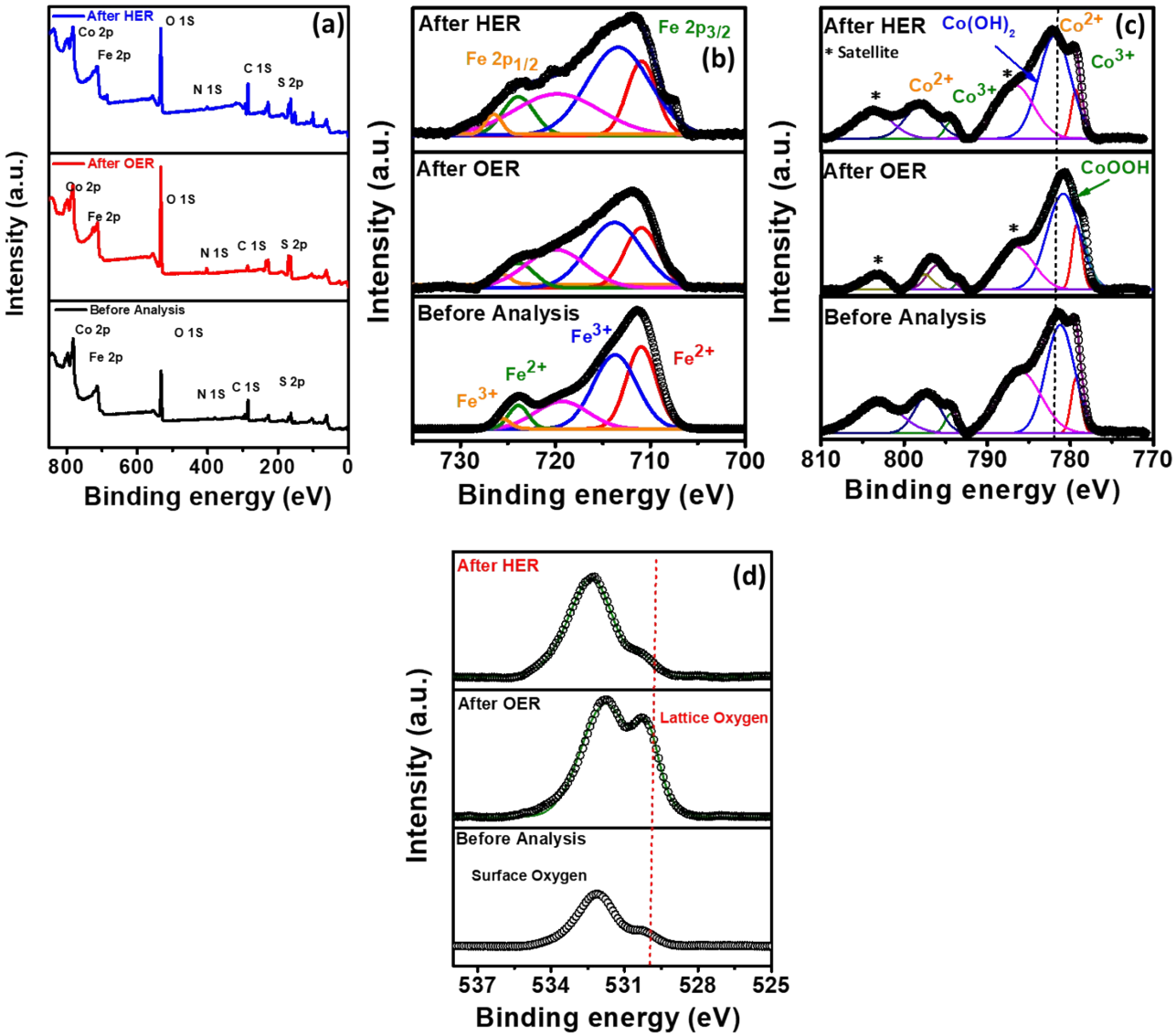

Fig. S27. (a) Survey spectrum and deconvulated XP spectra of , (b) Fe 2p, (c) Co 2p and (d) O 1s of CoFe(3:1)S_2 before and after HER and OER.

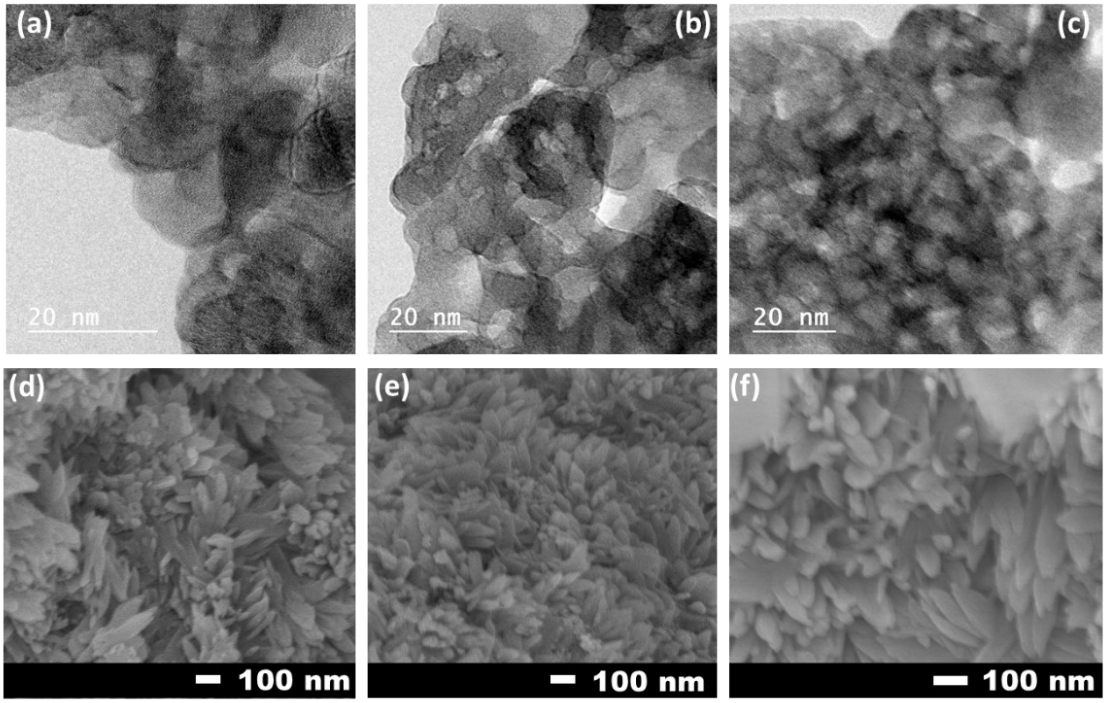

Fig. S28. TEM and SEM images of CoFe(3:1)S_2 after (a) & (d) after HER, (b) & (e) after OER in 1 M KOH and (c) & (f) after ORR in 0.1 M KOH.

Table S2: Literature reports showing the self powered water splitting with Zn air batteries:

Catalyst	η@10 mA cm^{-2} in 1.0 M KOH (V)		$E_{1/2}$ ORR (V)	ΔE (V)	ΔE cell (V)	pH universal HER activity	Zn-Air battery		Ref
	OER	HER					Power density (mW cm^{-2})	Specific capacity (mAh g^{-1})	
C_{60}-SWCNT	0.46	**0.38 (0.1 KOH) 0.33(PBS) 0.32 (0.5 M H_2SO_4)**	0.79	0.77	1.68	**yes**	NA	NA	2
FeCo/Co_2P	0.28	0.26	0.79	0.77	1.68	No	154		3
CoSA/N,S-HCS	0.31	0.17	0.85	0.67	1.64	No	173	781	4
$Ni_{0.5}Fe_{0.5}$@NG	0.21	0.35	0.83	0.61	1.69	No	85	765	5
NiS_2 /CoS_2–O NWs	0.24	0.18	0.70		1.77	No			6
CoN_x/NGA	0.3	198	0.83	0.70	1.71	No		638	7
NiFe/NCNF/CC	0.26		0.79	0.70	2.05	No	141	640	8
CoO_x@NOC	0.32	0.25	0.86	0.69	1.51	No	141.65	757	9
RuCo/NPC	0.35	0.21	0.80	0.79	1.68	No	79.4	1089	10
CoSA + Co_9S_8/ HCNT	0.33	0.25	0.85	0.75	1.59	No	177	788	11
$Ni_{1.9}FeS_{1.09}(OH)_{4.6}$	0.20	0.28@ 80 mA cm^{-2}			1.62	No	248		12
Cu-N-SC-1100	0.33	0.17	0.89	0.67	1.68	No	198	732	13
CoFe@NO –CNT	0.16	0.13	0.84	0.73	1.57	No	142	819	14
N, Co-CNTs	0.30	0.20	0.85		1.69	No	114		15
CoP@PNC-Do	0.32	0.17 (I M KOH) 0.16 (0.5M H_2SO_4)	0.80		1.74		138	730	16
CoFe(3:1)S_2 Our work	**0.25**	**0.117 1 M KOH 0.12 1 M PBS 0.98 0.5 M H_2SO_4**	**0.87**	**0.61**	**1.58**	**Yes**	**387**	**841**	This Work

References:

1. N. Thakur, M. Kumar, S. D. Adhikary, D. Mandal and T. C. Nagaiah, *Chem. Commun.*, 2019, **55**, 5021-5024.
2. R. Gao, Q. Dai, F. Du, D. Yan and L. Dai, *J. Am. Chem. Soc.*, 2019, **141**, 11658-11666.
3. Q. Shi, Q. Liu, Y. Ma, Z. Fang, Z. Liang, G. Shao, B. Tang, W. Yang, L. Qin and X. Fang, *Adv. Energy Mater.*, 2020, **10**, 1903854.
4. Z. Zhang, X. Zhao, S. Xi, L. Zhang, Z. Chen, Z. Zeng, M. Huang, H. Yang, B. Liu and S. J. Pennycook, *Adv. Energy Mater.*, 2020, **10**, 2002896.
5. P. Liu, D. Gao, W. Xiao, L. Ma, K. Sun, P. Xi, D. Xue and J. Wang, *Adv. Funct. Mater.*, 2018, **28**, 1706928.
6. J. Yin, Y. Li, F. Lv, M. Lu, K. Sun, W. Wang, L. Wang, F. Cheng, Y. Li and P. Xi, *Adv. Mat.*, 2017, **29**, 1704681.
7. H. Zou, G. Li, L. Duan, Z. Kou and J. Wang, *Appl. Catal. B: Environ.*, 2019, **259**, 118100.
8. C. Lai, J. Fang, X. Liu, M. Gong, T. Zhao, T. Shen, K. Wang, K. Jiang and D. Wang, *Appl. Catal. B: Environ.*, 2021, **285**, 119856.
9. M. E. Hilal, H. A. Younus, S. Chaemchuen, S. Dekyvere, X. Zen, D. He, J. Park, T. Han and F. Verpoort, *Catal. Sci. Technol.*, 2021.
10. Y. Pei, W. He, M. Wang, J. Wang, T. Sun, L. Hu, J. Zhu, Y. Tan and J. Wang, *Chem. Commun.*, 2021, **57**, 1498-1501.
11. Y. Li, R. Cao, L. Li, X. Tang, T. Chu, B. Huang, K. Yuan and Y. Chen, *Small*, 2020, **16**, 1906735.
12. B. Wang, C. Tang, H. F. Wang, B. Q. Li, X. Cui and Q. Zhang, *Small Methods*, 2018, **2**, 1800055.
13. M. Wang, K. Su, M. Zhang, X. Du and Z. Li, *ACS Sustain. Chem. Eng.*, 2021.
14. M. Li, S. Chen, B. Li, Y. Huang, X. Lv, P. Sun, L. Fang and X. Sun, *Electrochim. Acta*, 2021, **388**, 138587.
15. Q. Jin, B. Ren, H. Cui and C. Wang, *Appl. Catal. B,* 2021, **283**, 119643.
16. Y. Li, Y. Liu, Q. Qian, G. Wang and G. Zhang, *Energy Storage Mater.*, 2020, 28, 27-36.